Novel polyethylene/tungsten oxide/bismuth trioxide/barium sulfate/graphene oxide nanocomposites for shielding against X-ray radiations

T. Abdolahzadeh, J. Morshedian*, S. Ahmadi

Department of Polymer Processing, Iran Polymer and Petrochemical Institute (IPPI), P.O. Box 14975/112, Tehran, Iran

► *Original article*

ABSTRACT

Background: High-energy beams, such as gamma rays and X-rays, have many applications in nuclear power plants, healthcare, aerospace, and medicine. Therefore, appropriate radiation protection of living bodies in nuclear science and industries is essential to shield humans against the aforementioned radiation. Utilizing shielding materials is a practical method to protect individuals from harmful radiation. ***Materials and Methods***: High-density polyethylene (HDPE)-based nanocomposites were prepared to perform as a shield against X-ray radiation by using various weight fractions of the tungsten oxide, barium sulfate, and bismuth trioxide (10, 15, 20, and 25 wt). Samples' shielding properties were experimentally studied with an X-ray tube at 50, 60, 80, and 120 kVp. ***Results***: The recorded results showed that with increasing the number of nanoparticles, the transmission factor and HVL values were decreased and the linear attenuation coefficient was increased significantly. SEM, EDX analysis, and TEM evaluated the morphological properties of the fabricated samples. Results revealed that the particle size of the used nanoparticles was in the 25-50 nm range. Thermal study of the prepared nanocomposites including ΔH_m, crystalline percentage (X_c), melting point (T_m) as well as the thermal stability of the nanocomposites were determined by using DSC, and TGA, respectively. ***Conclusion***: Samples including 20% and 25% wt of Bismuth trioxide, and Tungsten trioxide loaded on graphene oxide reached 12% and 10% transmission factor values, respectively.

INTRODUCTION

High-energy beams, such as gamma rays and X-rays, have many applications in nuclear power plants, healthcare, aerospace, and medicine. Therefore, appropriate radiation protection of living bodies in nuclear science and industries is essential to shield humans against the aforementioned radiation. Utilizing shielding materials is a practical method for protection from harmful radiation [1]. Lead plays a significant role in human protection against X-ray and gamma radiation during radiology operations [2, 3]. However, high toxicity, heavyweight, and other environmental hazards are the most disadvantages of using lead shields [4].

Polymer/metal oxide nanocomposites have attracted a lot of attention as an alternative to traditional shields due to their special properties such as lightweight instead of various classifications of utilized materials for shielding [5], polyethylene-based composite is well organized in the absorption of high-energy beams [6, 7]. On the other hand, polyethylene has low price, is non-toxic, and recyclable [8].

Polyolefins such as polyisoprene, polyethylene,

polypropylene, *etc.*, due to C-C bonds in their structure, have high chemical stability. Nanocomposites with improved mechanical/ chemical properties can be obtained by introducing nanometal fillers into these materials. Moreover, adding fillers with shielding performance to polyolefin-based matrix leads to achieving nanocomposite materials with shielding application against x and gamma [5, 6]. Maahmoud *et al.* prepared composites of high-density polyethylene loaded with 10% and 50% lead oxide [9]. Under the research, high-density polyethylene filled with lead oxide nanocomposite has a minor impact on the matrix of the polymer. Eren *et al.* used low linear density polyethylene as a polymer matrix and used various weight fractions of lead oxide and tungsten oxide to synthesize shielding composite against X-ray and gamma radiations [10]. According to the reports of Kaloshkin *et al.*, γ-ray protection is based on ultra-high molecular weight polyethylene composites filled with boron carbide (B_4C) and nano tungsten oxide. They showed thatthere was a relationship between the weight fraction of nanoparticles and the gamma-ray attenuation coefficient values [11]. Laurenzi *et al.* used numerical studies to evaluate the

radiation properties of nanocomposites with a medium-density polyethylene and the effect of different polymer additives on the mechanism of shielding [12]. The authors reported that polyethylene reduces radiation power via simulated radiation sources.

Afshaar *et al.* considered the X-ray and gamma radiation attenuation properties of polyethylene-based composites filled with tungsten-molybdenum sulfide particles. They showed that high-density polyethylene loaded 45% tungsten composite has considerable shielding performance against X and gamma rays in term of heaviness and density compared to the pure lead sheets [13].

Here, high-density polyethylene-based nanocomposites filled with various weight fractions of the $BaSO_4$, Bi_2O_3, and WO_3 (10, 15, 20, and 25 % wt.) were prepared and their shielding efficiency against X-ray radiation was investigated by various techniques in radiology energy ranges. High-density polyethylene as a polymer matrix compared to other polymers has considerable properties including low cost, easy process capability, high mechanical properties, high crystallinity, and biocompatibility. Prepared high-density polyethylene-based shields can be used in radiology applications such as aprons and shield sheets [13].

Applied multi-step method included supporting nanofillers on nanographene oxide promoted the attenuation efficiency of the prepared composites. It could be realized that supporting GO with mentioned nanofillers led to perfect dispersion and distribution of nanofillers in the polymeric matrix. Here, high density polyethylene-based nanocomposites filled with different weight fractions of the Tungsten trioxide, Bismuth trioxide, and Barium sulfate (10, 15, 20, and 25 % wt.) were fabricated and their shielding attenuation performance against X-ray radiations were evaluated by different techniques. Utilizing high density polyethylene as a polymeric matrix was due to its special characteristics, such as easy processability, biocompatibility, low cost, and high mechanical characteristics. Prepared polyethylene-based shields have the potential to use in the radiology range (40kVp-120kVp) and are employed in medical applications.

MATERIALS AND METHODS

Materials

For preparing graphene oxide (GO), GO-tungsten-bismuth, and GO-barium nanoparticles, the $KMNO_4$, H_3PO_4, H_2SO_4, ethanol, H_2O_2, graphite, NH_3, acetone, and HCl were prepared from Merck & Co., Inc. Nano tungsten-oxide particles with 30 nm average size was obtained from Nanosany corporation, Lewiston, USA. Nano Barium sulfate was supplied by Sigma-Aldrich Co. (USA) and used without further purification. Zibo jiashitai technology Co (China) supplied Nano

Bismuth oxide metal powder. Injection grade of high-density polyethylene (52518) was prepared from Jam Petrochemical Co. (Bushehr, Iran).

Synthesis of graphene oxide

To synthesize GO, the method of Hummer was modified. For this purpose, 2L of H_2SO_4 was injected into a bottom flask and stirred at 300 rpm. Then, 50 g of $KMNO_4$ was subjoined to the H_2SO_4. Then, 10 gr of graphite was leisurely added to the suspension. Then, by adding 110 ml of H_3PO_4 to the previous suspension, the suspension was stirred for 72 hours (500 rpm) with concurrent heating (50 °C). Afterward, the suspension was then poured into a vacuum flask which was attached to ice. After adding 10 ml of H_2O_2 to the suspension, the vacuum flask was accumulated with deionized water. For sediment deposition, the suspension remained constant for 48 hours. Then, by filtrating the suspension, the remaining particles on the filter paper were washed with HCl to eliminate metal ions. At this stage, the suspension was washed with ionized water to negate the pH. Finally, in a heating furnace, the obtained material was dried for 1 hour at 80 ° C and then situated in a moisture reduction chamber for 48 hours [14].

Decoration of bismuth and tungsten oxide on GO (WO_3-Bi_2O_3-GO)

By adding 1 gr of GO to 100 mL of ethanol, the obtained mixture was ultrasonicated for 10 min at 50 °C. Then, by adding the ethanol and graphene oxide suspension, 5 gr of WO_3, and 5 gr of Bi_2O_3 were added up to 250 ml of deionized H_2O, and the resulting mixture was reacted at 60 °C for 0.5 hr. In the next step, 10 ml of HCl and 40 ml of NH_3 were injected into a round-bottom flask. The resulting suspension was stirred at 80 °C for two days. The particles were then rolled up by filtering and then washing with deionized H_2O. Finally, the WO_3-Bi_2O_3-GO labeled fillers (resulting fillers) were dried at 100 °C [14]. This method was used to provide complete support of nanotungsten oxide and bismuth trioxide on nanographene oxide (see figure 1).

Decoration of barium sulfate with GO (BaSO4-GO)

By adding 1 gr GO to 100 ml ethanol, the obtained mixture was ultrasonicated for 10 min at 50 °C. Then, mentioned ethanol-GO suspension and 10 gr $BaSO_4$ were added to 250 ml of deionized H_2O, and the obtained mixture reacted at 60 °C for 0.5 hr. Then, 10 ml of HCl and 40 ml of NH_3 were injected into a round-bottom flask. For two days, the suspension was stirred at 80 °C. The fillers were then gathered by filtering and washing with deionized H_2O. The particles were then rolled up by filtering and washing with deionized H_2O. Finally, the labeled $BaSO_4$-GO sample dried at 100 °C. This method was utilized to obtain optimized dispersion and distribution of nanoparticles in the polymer [16].
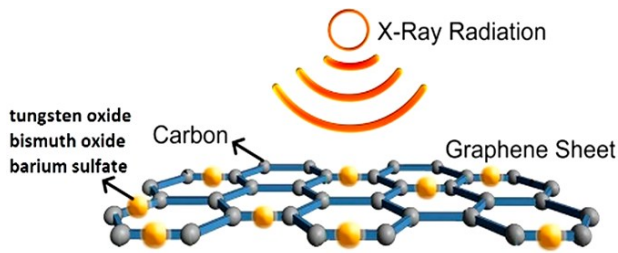
Figure 1. Decoration of utilized nanoparticles on nanographene oxide sheets and its performance against X-ray radiations.

Nanocomposite samples preparation

40g of polyethylene with various weight percentages of nanoparticles decorated on nanographene oxide including 0, 10, 15, 20, and 25% were blended in an internal mixer at 80 rpm for 10 minutes at 200 °C. mentioned synthesized samples were made by the melt blending technique [14].

Table 1. Composition of the prepared nanocomposite samples.

Sample No.	Sample name	Composition		
		WO3/Bi$_2$O$_3$/GO (wt. %)	HDPE (wt. %)	BaSO$_4$-GO (wt. %)
1	PE-0	0	100	0
2	PE-A-10	10	90	0
3	PE-A-15	15	85	0
4	PE-A-20	20	80	0
5	PE-A-25	25	75	0
6	PE-B-10	0	90	10
7	PE-B-15	0	85	15
8	PE-B-20	0	80	20
9	PE-B-25	0	75	25

Characterization

FT-IR spectroscopy analysis was performed by using Thermo Science, NICOLET IS5 (USA) infrared spectrophotometer. The morphology of the prepared samples was examined by using transmission electron microscopy (TEM) (EM2085, Philips, Netherlands) and VEGA scanning electron microscope (SEM) (TESCAN, Czech Republic). Differential scanning calorimetry (DSC) was done on DSC Q 1000 TA (USA) under N2 atmosphere at a 10%/min heating rate. Crystallization degree (Xc) and Melting temperature (Tm) were obtained through the first heating scan Thermogravimetric analysis (TGA) to evaluate the thermal stability of the samples in the 25-600 °C temperature range using TGA/DSC1 (Mettler Toledo Inc., Switzerland) under N2 atmosphere with a 10 °C /min heating rate. The prepared nanocomposites' linear attenuation coefficients (μ) were obtained using X-ray tube (micro –CT imaging using LOUTUS-NDT, three experiments were conducted for each sample) [15]. The value of μ is obtained by using equation (1).

$$\mu = \frac{1}{x} Ln \frac{I_0}{I} \qquad (1)$$

Where I_0 is the original intensity, I is the intensity at depth of x and μ is the linear attenuation coefficient and x is the thickness of the samples.

Mass attenuation coefficient values (μ/ρ) were obtained by utilizing linear attenuation coefficient parameters. An X-ray tube radiometer was used to measure the amount of absorbed dose, which can produce up to 1200 keV photons. The sample preparation procedure was based on ISO/IEC 17025. The Mentioned machine can count passing beams through the samples, therefore the number of absorbed rays is obtained from Eq. (2).

$$\text{Transmission factor} = (C/C_0) \times 100 \qquad (2)$$

Where C_0 is the primary radiation count, C is the passed number, and the irradiation time is 180 s.

The prepared samples' heaviness was calculated by employing equation 3, in which the heaviness values of the prepared samples were calculated by using equation (3) and lead is considered as a standard and the synthesized composite samples related to lead were normalized (three experiments were conducted for each sample) [16].

$$\% \text{ Heaviness} = \frac{\text{density of the given material}}{\text{density of lead}} \times 100 \qquad (3)$$

The effectiveness of shielding materials could be explained by the half value layer (HVL). HVL is the thickness of a substance that can reduce the intensity of radiation to half of its original value

$$x_{1/2} = \frac{Ln2}{\mu} \qquad (4)$$

In addition, for each sample, the equivalent lead thickness was obtained using the Beer-Lambert equation [17]:

$$(\mu/\rho)_{Sample} \times \rho_{Sample} \times X_{Sample} = (\mu/\rho)_{Lead} \times \rho_{Lead} \times X_{Lead} \qquad (5)$$

Where ρ_{Sample}, $(\mu/\rho)_{Sample}$, $_{Sample}$, ρ_{Lead}, $(\mu/\rho)_{Lead}$ and, x_{Lead} are density of the sample, total mass attenuation of the sample (with coherent scattering), the thickness of sample, density of lead, total mass attenuation of lead, and thickness of pure lead, respectively.

Statistical analysis

The statistical analysis was done with origin pro 8 software. Mean ± standard deviation was declared for ordinal data. Obtained parameters were investigated within the number of irradiated and transmitted rays between groups by employing one-way ANOVA. p <0.05 was measured statistically.

RESULTS

FT-IR study of the BaSO$_4$, GO, Bi$_2$O$_3$, WO$_3$/Bi$_2$O$_3$/GO and BaSO$_4$/GO

To study the complete decoration of WO$_3$ and Bi$_2$O$_3$ on the surface of GO, FTIR spectroscopy was utilized. Received spectrums for GO, WO$_3$, Bi$_2$O$_3$, and WO$_3$/Bi$_2$O$_3$/GO have been shown in figure 2A. Based on the recorded spectrum of GO, the bonds at 1725, and 1630 cm^{-1} are relevant to the C=O, and C=C bonds

of carboxylic groups and aromatic rings, respectively, and observed peaks at 1200, and 1050 cm^{-1} are due to the C-O bonds in alcohols and epoxide groups [14]. In the obtained spectrum, sharp peaks at 2900 and 2800 cm^{-1} are due to C-H stretching vibration [18]. This result was a proof of successful synthesizing of GO. In addition, FTIR analysis for WO_3/Bi_2O_3 (T-B-G) has been shown in figure 2 B as well.

To investigate decoration of $BaSO_4$ on the surface of GO, FTIR spectroscopy was utilized (see figure 2B). As shown, $BaSO_4$ represented all of the needed functional groups for bonding on graphene oxide. By investigating on the spectrum of GO, $BaSO_4$, and $BaSO_4/GO$, it can be seen that, the intensity of the above peaks in BaSO4/GO (Ba-GO) wereless than graphene oxide and $BaSO_4$. So, it is an evidence for the reaction between functional groups of Bi_2O_3 by the same functional groups on the nanographene oxide [14].
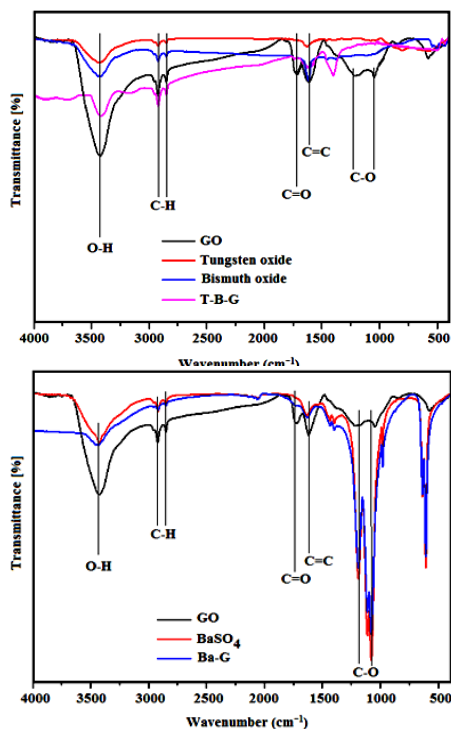

Figure 2A. FT-IR spectrums of GO, $Bi_2O_3WO_3$, GO/WO3/Bi_2O_3, **B)** FT-IR spectrums of GO, $BaSO_4$ and $BaSO_4/GO$.

Table 2. Main FT-IR peaks of GO, Bi_2O_3, WO_3, $BaSO_4/WO_3/$ Bi_2O_3/GO and $BaSO_4/GO$.

Wavenumber (cm^{-1})	Information of peak
1630	C=C stretching vibration
3200-3600	O-H stretching vibration
1050, 1200	C-O stretching vibration
1725	C=O stretching vibration
2800, 2900	C-H stretching vibration

Shielding characterization of synthesized nanocomposite samples
Investigating attenuation properties of samples in the exposure of X- rays

The recorded results for the shielding effectiveness of the fabricated samples are shown in

table 3. X-ray tube in the 50, 60, 80,120 kVp energy range for radiology application was utilized in this analysis [14,19]. Obtained results illustrated that the mass and linear coefficient values were increased by nanoparticles' weight fraction enhancement.WO$_3$/ Bi_2O_3-based nanocomposites represented higher µ values due to their superior atomic number compared to $BaSO_4/GO$-based samples.

By utilizing linear attenuation coefficient values from eq 4, the HVL value was calculated. Recorded results for HVL values were collected in table 4. Under the table 3 results, the linear attenuation coefficient values of the fabricated nanocomposites were increased by density enhancement in the fabricated nanocomposites. Therefore, HVL values were reduced by loading more nanoparticles in the prepared sample [14,20]. On the other hand, increase in energy intensity led to decrease in the shielding efficiency of the nanocomposite samples, therefore, the best result was expected in 50 kvp.

Table 3. Attenuation results of the synthesized nanocomposite samples with two different thicknesses by employing four different energy values.

Sample	Energy (kVp)	Linear attenuation µ(mm^{-1}) Thickness (2 mm)	Thickness (6 mm)	Density (g/cm^3)	Mass attenuation µ/ρ (mm^{2}g^{-1}) Thickness (2 mm)	Thickness (6 mm)	statistical analyses
PE-0	50	0.09	0.07	0.95	0.1	0.08	p<0.05
	60	0.08	0.06		0.09	0.07	p<0.05
	80	0.07	0.05		0.08	0.06	p<0.05
	120	0.05	0.04		0.06	0.04	p<0.05
PE-A-10	50	0.37	0.24	1.29	0.28	0.18	p<0.05
	60	0.33	0.22		0.25	0.17	p<0.05
	80	0.28	0.17		0.22	0.13	p<0.05
	120	0.2	0.13		0.15	0.1	p<0.05
PE-A-15	50	0.68	0.35	1.33	0.51	0.26	p<0.05
	60	0.6	0.31		0.45	0.23	p<0.05
	80	0.79	0.25		0.59	0.19	p<0.05
	120	0.35	0.18		0.26	0.13	p<0.05
PE-A-20	50	0.72	0.36	1.38	0.52	0.27	p<0.05
	60	0.64	0.32		0.46	0.23	p<0.05
	80	0.52	0.26		0.38	0.18	p<0.05
	120	0.37	0.19		0.27	0.14	p<0.05
PE-A-25	50	0.85	0.38	1.43	0.59	0.26	p<0.05
	60	0.76	0.35		0.53	0.24	p<0.05
	80	0.61	0.29		0.42	0.2	p<0.05
	120	0.44	0.22		0.64	0.15	p<0.05
PE-B-10	50	0.23	0.16	1.06	0.21	0.15	p<0.05
	60	0.21	0.14		0.2	0.13	p<0.05
	80	0.18	0.12		0.17	0.11	p<0.05
	120	0.13	0.09		0.12	0.08	p<0.05
PE-B-15	50	0.27	0.2	1.1	0.24	0.18	p<0.05
	60	0.26	0.18		0.23	0.16	p<0.05
	80	0.23	0.16		0.21	0.14	p<0.05
	120	0.2	0.13		0.18	0.12	p<0.05
PE-B-20	50	0.32	0.21	1.2	0.27	0.17	p<0.05
	60	0.29	0.19		0.24	0.16	p<0.05
	80	0.24	0.16		0.2	0.13	p<0.05
	120	0.18	0.12		0.15	0.1	p<0.05
PE-B-25	50	0.42	0.26	1.27	0.33	0.2	p<0.05
	60	0.39	0.23		0.31	0.18	p<0.05
	80	0.32	0.2		0.26	0.15	p<0.05
	120	0.25	0.18		0.2	0.14	p<0.05

Table 4. Half value layer (HVL) result of the fabricated nanocomposite samples with a thickness value of 6 mm by employing four different energy values.

HVL (cm)	PE-0	PE-A-10	PE-A-15	PE-A-20	PE-A-25	PE-B-10	PE-B-15	PE-B-20	PE-B-25
50kVp	10	2.92	2	1.94	1.84	4.37	3.5	3.33	2.69
60kVp	11.7	3.18	2.26	2.18	2	5	3.89	3.68	3.04
80kVp	14	4.12	2.8	2.69	2.41	5.83	4.37	4.37	3.5
120 kVp	17.5	5.38	3.89	3.68	3.18	7.78	5.38	5.83	3.89

Transmission factor results of synthesized nanocomposite samples

Tungsten, Bismuth, and Barium-based nanocomposites due to their absorbing dose potential have various applications as a shield. To investigate the absorption characteristics of synthesized samples, the transmission factor analysis was employed (figure 3). The results of figure 3 were generated based on the optimized situation: the voltage was 50, 60, 80, and 120 kVp, the irradiation time around 180 s and the current of 200 mA. Figure 3 a, b, c, and d are related to the absorbed dose values of the synthesized samples at 50, 60, 80, and 120 kVp, respectively. As it can be seen in the all series, prepared samples containing tungsten and bismuth oxide (WO$_3$/Bi$_2$O$_3$/GO) had shown much higher absorbed dose and, as a result lower transmission factor values in comparison with barium sulfate (BaSO4-GO) based nanoparticles.
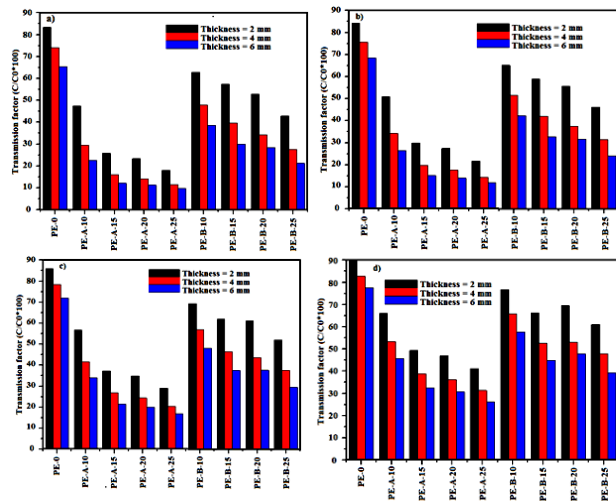

Figure 3. Transmission factor values of the synthesized nanocomposite samples with three thickness values of 2, 4, and 6 mm at the four employed energy values including: **a)** 50 kvp, **b)** 60 kvp, **c)** 80 kvp, **d)** 120 kvp.

Equivalent lead thickness can express the effectiveness of X-ray shielding materials [17]. This section appraised the equivalent lead thickness values of obtained nanocomposite samples According to the Eq.5 to compare their efficiency against X-ray radiation. Figure 4 demonstrated the effect of thickness and particle weight fraction on their equivalent lead thickness. Increasing nanoparticles'

weight fraction and the samples' thickness led to enhancement in their equivalent lead thickness values. On the other side, WO$_3$/Bi$_2$O$_3$-based nanocomposites revealed higher equivalent lead thickness values compared to BaSO$_4$/GO-based nanocomposites [21, 22].
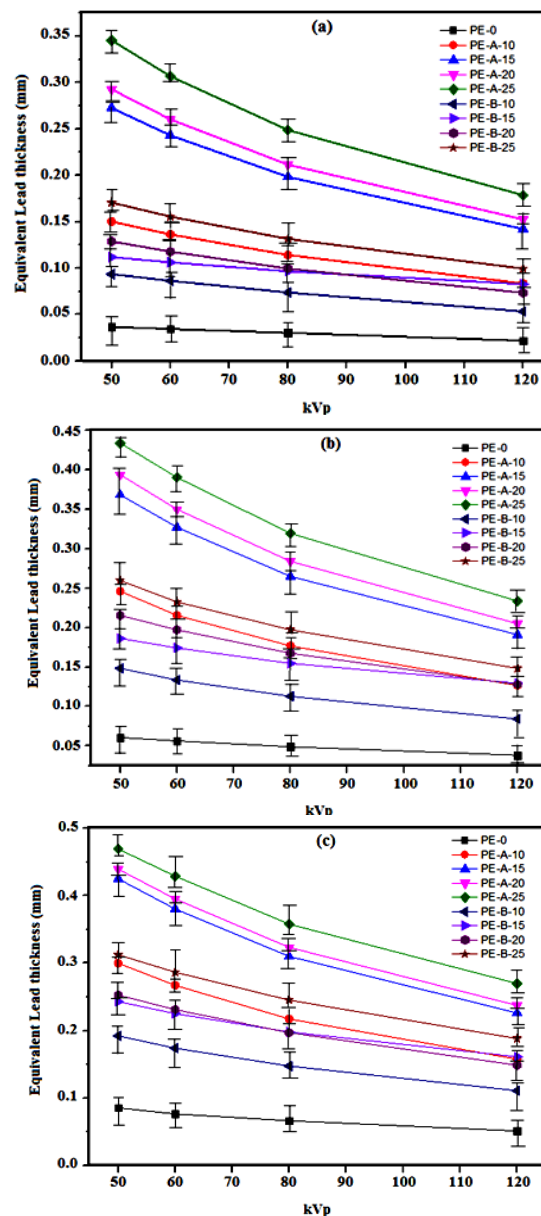

Figure 4. Measured equivalent lead thickness (mm) of the fabricated nanocomposite samples in four different energy values at **a)** thickness = 2 mm **b)** thickness = 4 mm and **c)** thickness = 6 mm.

Heaviness results of synthesized nanocomposite samples

The density and heaviness values of the prepared nanocomposite samples were calculated and the obtained results were gathered as a brief result in figure 5, and table 5. According to the obtained results, the fabricated shield samples were so light compared to the commercial Pb-based samples [16].
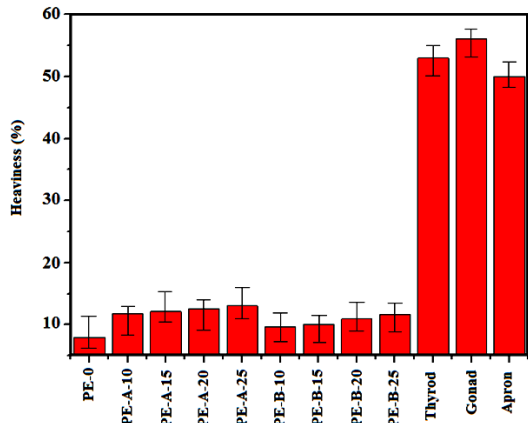
Figure 5. Heaviness values of the synthesized nanocomposite samples.

Table 5. Heaviness result of the synthesized nanocomposite samples.

Sample	Heaviness (%)	Reference
PE-0	7.96	This work
PE-A-10	11.77	
PE-A-15	12.11	
PE-A20	12.54	
PE-A-25	13.05	
PE-B-10	9.66	
PE-B-15	10	
PE-B-20	10.93	
PE-B-25	11.61	
Thyroid	53	[19]
Gonad	56	[19]
Apron	50	[19]
Concrete	20	[23]
Rubber+50 wt% lead	24	[24]
Aluminum A356	24.27	[25]

Morphology of the fabricated nanocomposite

SEM microscope was used for morphological characterization of the prepared nanocomposites. In addition, EDX maps of Tungsten, Bismuth, and Barium atoms for the samples containing 15 and 20% of nanoparticles are shown in figure 6. According to the recorded maps, the distribution and dispersion of the used fillers were completely done in the polymer bed.

To further morphological study of the prepared nanocomposite samples, TEM photos of the nanocomposites containing 10 wt% of nanoparticles was recorded and the obtained photos were explained in figure. 8. As it can be seen, the employed fillers were completely dispersed in the polymer media, which could be due to the efficacious supporting of the nanoparticles on graphene surfaces. According to the figure.7 photos, employed nanoparticles had particle sizes in the range of 25-50 nm.

Thermal characterization of the synthesized nanocomposite samples

The thermal stability of the prepared nanocomposites was studied by TGA. The recorded curves were depicted in figure 9 and the achieved results were gathered as a brief conclusion in Table 6. Interestingly maximum weight loss temperature (T_{max}) were measured to be at 427, 470, 471, 472, 473, 477, 477, 477, and 476 °C for sample one to eight, respectively. These results indicated that introducing employed nanoparticles to the polymeric matrix led to increasing thermal resistance behavior [20]. So, the weight percentages of used nanoparticles had a direct relationship with the thermal stabilities of the fabricated nanocomposites [20]. Finally, the char yield amount at 600 °C was calculated to be at 0, 11, 15, 18, 25, 8, 11, 14, and 21% for sample one to eight, respectively.
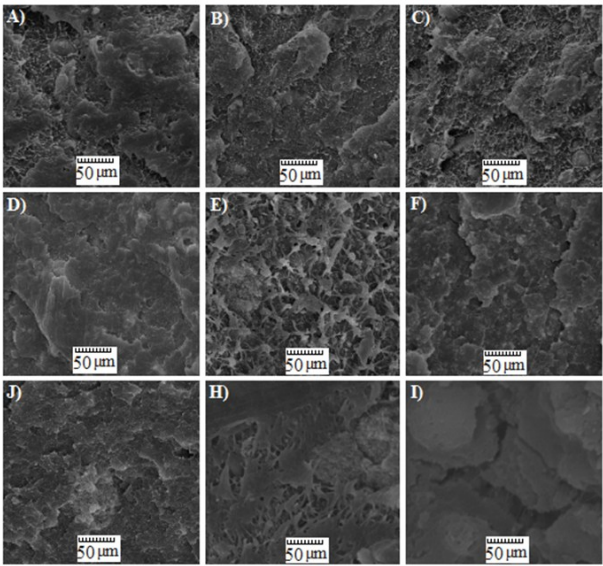

Figure 6. SEM images of **A)** PE-A-10, **B)** PE-A-15, **C)** PE-A-20, **D)** PE-A-25, **E)** PE-B-10, **F)** PE-B-15, **J)** PE-B-20, **H)** PE-B-25, and **I)** PE-0.
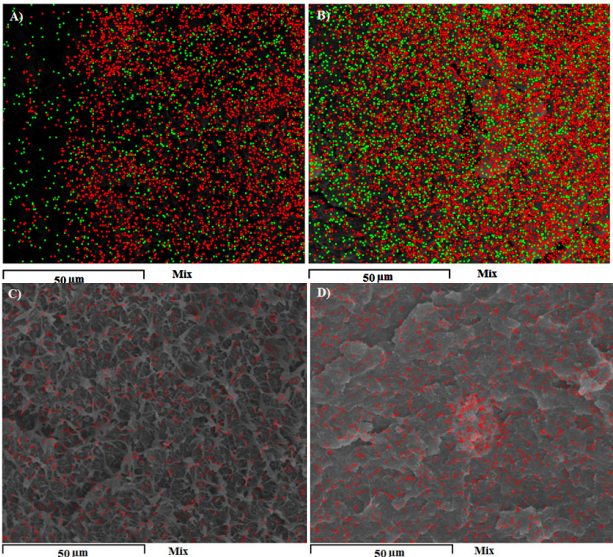

Figure 7. EDX mapping of **A)** PE-A-15, B) PE-A-20, **C)** PE-B-15, and **D)** PE-B-20. At the pictures of A and B, Tungsten and Bismuth atoms were shown in green and red colors, respectively; in the pictures of C and D, the Barium atoms were shown in red colors.
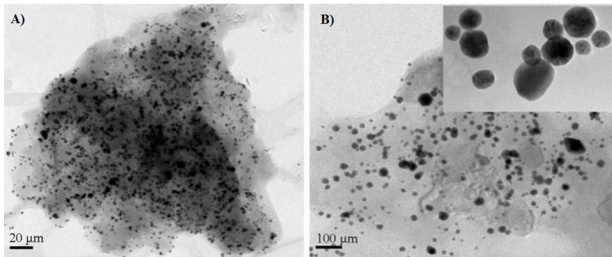
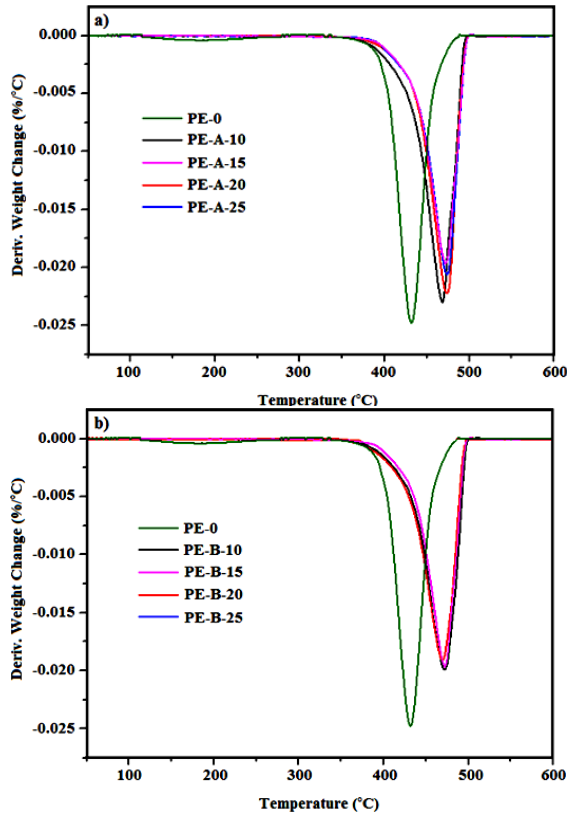**Figure 8.** TEM photos of A) PE-A-10, B) PE-B-10.

Figure 9. DTGA curves of the prepared nanocomposite samples.

Table 6. Thermal properties of the prepared nanocomposite samples.

Sample	TGA		DSC		
	Tmax (°C)a	Char yield (%)b	ΔH_m (J/g)	X_c (%)	T_m (°C)
PE-0	427	0	189.4	65.7	131.4
PE-A-10	470	11	157.2	54.6	131.1
PE-A-15	471	15	156.5	54.3	130.7
PE-A-20	472	18	141.9	49.2	131.3
PE-A-25	473	25	136.7	47.5	131.1
PE-B-10	477	8	173.1	60.1	132.1
PE-B-15	477	11	167.2	58	131.2
PE-B-20	477	14	165.1	57.3	130.9
PE-B-25	476	21	151.7	52.7	131

Thermal properties of the produced nanocomposites were extracted from DSC thermograms (figure 10), and obtained results including ΔH_m, melting point, and percentage of crystalline polymer, X_c, have been gathered as a brief conclusion in table 6. According to the data in table 6, produced nanocomposite samples by employing 10, 15, 20, and 25% nanoparticles had less crystallinity percentage in comparison with the unfilled PE [30]. Neat PE showed 65.7 %. In X_c values

By adding 10% of $WO_3/Bi_2O_3/GO$ and $BaSO4$-GO nanoparticles, X_c of the samples decreased to 54.6, and 60.1 %, respectively. However, by a further increase in the nanoparticles amount up to 25%, the X_c values were declined related to the neat PE and reached 47.5, and 52.7 % for PE-A-25, and PE-B-25, respectively. According to the depicted curves in figure 10, prepared nanocomposite samples had narrow variations in T_m values, where all of the samples had T_m values in the range of 130.7-132.1°C.
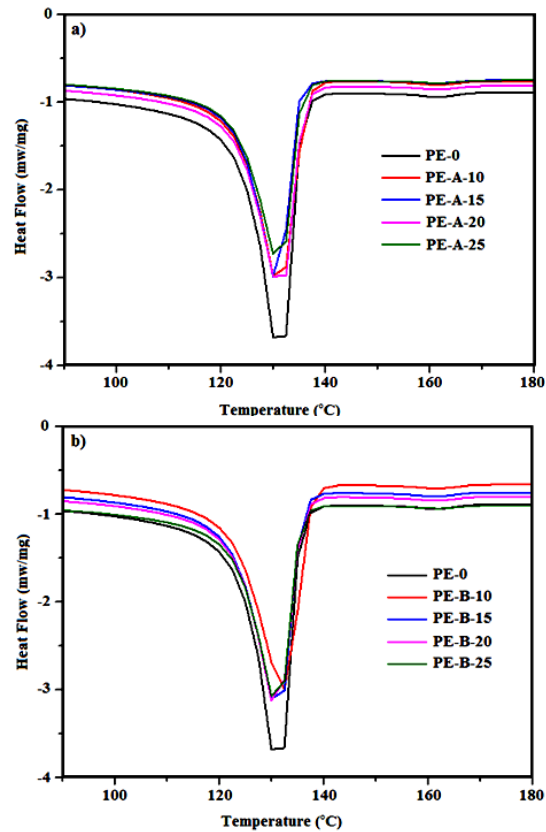

Figure 10. DSC curves of the prepared nanocomposite samples.

DISCUSSION

According to the FT-IR results in figure 2, Tungsten oxide, and Bismuth oxide include all of the necessary functional groups for bonding on the GO (see table 2 results). The existence of similar peaks in GO, Tungsten oxide, and Bismuth oxide confirms the possibility of the molecular attachment between mentioned materials [14,17]. By evaluating FTIR spectrum of GO, WO_3, Bi_2O_3 and, $WO_3/Bi2O3/GO$, it can be found that the OH group of $WO3/Bi2O3/GO$ has less intensity in comparison with WO_3, Bi_2O_3, and GO. These results confirm the successful reaction between GO, WO_3, and Bi_2O_3 via hydroxyl groups as it was repeatedly reported in the literature [14,17].

According to the table 3 results, the density of the fabricated samples was increased by increasing weight fractions of the employed $WO3$, Bi_2O_3, and $BaSO_4$ nanoparticles. Recorded results demonstrated that, the mass attenuation parameters shifted to

higher values by loading more nanoparticles. According to the reported data in the academic reports, the mentioned trend can be due to the increasing nanoparticles weight fractions and filler dispensability of the polymer matrix as well. Mentioned analysis emphasizes the better performance of nanocomposite samples at all the X-ray energy ranges rather than polymer matrix alone [9].

Achieved data demonstrated that the transmission factor values had direct relationship with nanoparticles' weight fractions. Furthermore, lower transmission factor values were obtained at lower voltage values (50 kVp). Figure 3 illustrates that the fabricated nanocomposite samples have transmission factor in the close range with the commercial shielding aprons where, PE-A-25 as a synthesized nanocomposite (6mm thickness) and Thyroid, Gonad, and Apron as commercial shields represented transmission factor of 10, 8, 3, and 1 % at 50kVp, respectively [19].

According to the equivalent lead thickness results, the sample PE-A-25 with 6 mm thickness showed the equivalent lead thickness approximately equal to 0.05 mm of pure lead. These achievements were a confirmation that the employed method to synthesize and characterization of the nanocomposite samples compared to lead as a benchmark was suitable and proves the sample's performance against X-ray.

According to equation 1, in 50 keV, if we normalize the thickness of nanocomposite shielding samples to the commercial apron, obtained results illustrated that the sample PE-A-25 (thickness=6 mm) had the same attenuation behavior as the apron in (thickness =5.5 mm). This is another superiority of PE-A-25 nanocomposite sample. Fabricated nanocomposite samples in terms of thickness, heaviness, and shielding properties (radiology energy range) showed more efficiency than the commercial apron ones. On the other side, the employed polymer in this research demonstrated much more flexibility compared to the Pb-based shield. About heaviness, a fabricated nanocomposite sample with 25% $WO_3/Bi_2O_3/GO$ was 4.10 lighter than commercial shields. The most competitive priority of polymer nanocomposites is their lightness which made them a qualified alternative to other commercial shielding materials as reported in table 5 [19].

It can be acclaimed that, using Barium sulfate on GO ($BaSO_4$-GO) nanoparticles had more significant effect on improving thermal resistance characteristics of the synthesized nanocomposites samples compared to WO_3/Bi_2O_3 on Graphene oxide (tungsten oxide-bismuth trioxide) nanoparticles.

CONCLUSION

Here, PE-based nanocomposites of Bismuth trioxide, Barium sulfate, and Tungsten oxide were fabricated, and subsequently, their shielding efficiency of them was investigated. The obtained results showed that with increasing the weight fraction of the employed fillers, the linear and mass attenuation coefficient and the transmission factor values have increased significantly.

REFERENCES

1. Singh AK, Singh RK, Sharma B, Ajay Kumar Tyagi AK (2017) Characterization and biocompatibility studies of lead Free X-ray shielding polymer composite for healthcare application. *Radiation Physics and Chemistry,* **138**: 9-15.
2. Lyra M and Charalambattou P (2011) Radiation protection of staff in 111In radionuclide therapy- is the lead apron shielding effective? R*ad Prot Dosi,* **147**: 272–276.
3. Aral N, Nergis FB, Candan C (2015) An alternative X-ray shielding material based on coated textiles. Textile Research Journal, 86.
4. Maghrabi HA, Vijayan A, Mohaddes F, Deb P, Wang L (2016) Evaluation of X-ray radiation shielding performance of barium Sulphate-coated fabrics. *Fibers and Polymers,* **17**: 2047-2054.
5. Song Y, Phule AD, Wang D, Ma L, Zhang ZX (2021) Lightweight self-cleaning trans-polyisoprene/multiwalled carbon nanotubes open-cell composite material: Its electromagnetic shielding performance. *Express Polym Letters,* **15**: 865–877.
6. Xiao H, Zeng K, Hu J H, Yang G (2021) Multiple cooperative systems obtained by powder metallurgy-like processing method: Adenine containing phthalonitrile/graphene/Fe3O4 high-performance composites with ultra-high EMI shielding. *Express Polym Letters,* **15**: 791-807.
7. Adams J, Hathaway D, Grugel R, Watts J, Parnell T, Gregory J (2005) Revolutionary concepts of radiation shielding for human exploration of space. Book 211–218.
8. Nambiar S and Yeow JTW (2012) Polymer-composite materials for radiation protection. *ACS Appl Mater Interfaces,* **4**: 5717–5726.
9. Mahmoud ME, El-Khatib AM, Badawi MS, Rashed AR, El-Sharkawy RM, Thabet AA (2017) Fabrication, characterization and gamma rays shielding properties of nano and micro lead oxide-dispersed-high density polyethylene composites. *Radiation Physics and Chemistry,* **145**: 160-173.
10. Belgin EE and Aycik GA (2015) Preparation and radiation attenuation performances of metal oxide filled polyethylene based composites for ionizing electromagnetic radiation shielding applications. *J Radioanal Nucl Chem,* **306**: 107-117.
11. Kaloshkin SD, Tcherdyntsev VV, Gorshenkov MV, Gulbin VN, Kuznetsov SA (2012) Radiation-protective polymer-matrix nanostructured composites. *J Alloys Compd,* **536S**: S522– S526.
12. Laurenzi S, de Zanet G, Santonicola MG (2020) Numerical investigation of radiation shielding properties of polyethylenebased nanocomposite materials in different space environments. *Acta Astronautica,* **170**: 530–538.

13. Afshar M, Morshedian J, Ahmadi S (2019) Radiation attenuation capability and fow characteristics of HDPE composite loaded with W, MoS2, and B4C. *Polym Compos, 40: 149-158.*

14. Abdolahzadeh T, Morshedian J, Ahmadi S (2022) Preparation and characterization of nano WO3/Bi2O3/GO and BaSO4/GO dispersed HDPE composites for X-ray shielding application. *Polyolefins Journal, 3009: 1201.*

15. Akkurt I, Akyıldırım H, Mavi B, Kilincarslan S, Basyigit C (2010) Photon attenuation coefficients of concrete includes barite in different rate. *Annals of Nuclear Energy, 37: 910–914.*

16. Harish V and Harish NNH (2012) Lead oxides filled isophthalic resin polymer composite for gamma radiation shielding applications. *Ind J Pure App, Phys, 50: 847-850.*

17. Hashemi S A, Mousavi S M, Faghihi R, Arjmand M, Sina S, Amani AM (2018) Lead oxide-decorated graphene oxide/epoxy composite towards X-Ray radiation shielding. *Radiation Physics and Chemistry, 146: 77–85.*

18. Hanifpour A, Bahri-Laleh N, Nekoomanesh-Haghighi M, Karimi M (2017) Synthesis and characterization of poly1-hexene/silica nanocomposites. *Polym Test, 61: 27-34.*

19. Abdolahzadeh T, Morshedian J, Ahmadi S, Ay M R, Mohammadi O (2021) Introducing a novel Polyvinylchloride/Tungsten composites for shielding against gamma and X- ray radiations. *Iran J Nuc Med, 29: 58-64.*

20. Bagheri K and Razavi SM (2018) Thermal Resistance, Tensile Properties, and Gamma Radiation Shielding Performance of Unsaturated Polyester/Nanoclay/PbO Composites. *Radiation Physics and Chemistry, 146: 5-10.*

21. Baksi BG, Sen BH, Eyuboglu TF (2008) Differences in aluminum equivalent values of, endodontic sealers: conventional versus digital radiography. *J Endod, 34: 1101–1104.*

22. Mota EG, Rockenbach MIB, da Costa NP, Rigo A, Coelho CRR (2008) Radiopacity of impression materials using an indirect digital system. *Rev Odonto Ciência, 23: 333–337.*

23. Obaid SS, Gaikwad DK, Pawar PP (2018) Determination of gamma ray shielding parameters of rocks and concrete. *Rad Phys Chem, 144: 356-360.*

24. Mheemeed AK, Hasan HI, Al-Jomaily FM (2017) Gamma-ray absorption using rubber-lead mixtures as radiation protection shields. *J Radioanal Nucl Chem, 29: 653–659.*

25. Chen S, Bourham M, Rabiei A (2015) Attenuation efficiency of X-ray and comparison to gamma ray and neutrons in composite metal foams. Radiat Phys Chem, 117: 12-22.

26. Sertchook H, Elimelech H, Makarov C, Khalfin R, Cohen Y, Shuster M, Babonneau F, Avnir D (2007) Composite particles of polyethylene@ silica. *J Am Chem Soc, 129: 98.*

27. Dehghani-Sanijand AA and Blackburn RS (2008) IR study on hydrogen bonding in epoxy resin–silica nanocomposites. *Prog Nat Sci, 18: 801-805.*

28. Moseenkov SI, Kuznetsov VL, Kolesov BA, Zavorin AV, Serkova AN, Zolotarev NA (2021) Design of effective surface contacts on polymer composites modified with multiwalled carbon nanotubes. *Expres Polym Lett, 15: 826-838.*

29. Hanifpour A, Bahri-Laleh N, Nekoomanesh-Haghighi M (2020) Methacrylate functionalized POSS as an efficient adhesion promoter in olefin-based adhesives. *Polym Eng Sci, 60: 2991-3000.*

30. Mahmoud ME, El-Khatib AM, Badawi MS, Rashed AR, El-Sharkawy RM, Abouzeid A (2018) Thabet recycled high-density polyethylene plastics added with lead oxide nanoparticles as sustainable radiation shielding materials. *J Clean Produc, 176: 276-287.*